# Long-range order and thermal stability of thin Co2FeSi films on GaAs(111)B

B Jenichen, J Herfort, K Kumakura, A Trampert

# Long-range order and thermal stability of thin $Co_2FeSi$ films on GaAs(111)B

B. Jenichen,* J. Herfort, K. Kumakura,† and A. Trampert

*Paul-Drude-Institut fuer Festkoerperelektronik,*

*Hausvogteiplatz 5–7,D-10117 Berlin, Germany*

( Dated: 25th May 2010)

## Abstract

$Co_2FeSi$/GaAs(111)B hybrid structures are grown by molecular-beam epitaxy and characterized by transmission electron microscopy (TEM) and x-ray diffraction. The lattice matched $Co_2FeSi$ films grow in a three-dimensional island growth mode at substrate temperatures $T_S$ between $T_S = 100\,^{\circ}\mathrm{C}$ and $425\,^{\circ}\mathrm{C}$. The structures have a stable interface up to $T_S = 275\,^{\circ}\mathrm{C}$. The films contain fully ordered $L2_1$ and partially ordered $B2$ phases. The spatial distribution of long-range order in $Co_2FeSi$ is characterized using a comparison of TEM images taken with superlattice reflections and the corresponding fundamental reflections. The spatial inhomogeneities of long-range order can be explained by local non-stoichiometry due to lateral segregation or stress relaxation without formation of extended defects.

PACS numbers: 75.50 Bb, 81.15.Hi, 61.05.J-, 68.35.Ct

*bernd.jenichen@pdi-berlin.de

†Also at NTT Basic Research Laboratories, 3-1 Morinosato Wakamiya, Atsugi-shi, Kanagawa 243-0198, Japan.

## I. INTRODUCTION

There is an increasing interest in Heusler alloys as candidates for sources of spin injection into semiconductors [1–4]. The Heusler alloy $Co_2FeSi$ is a ferromagnetic half-metal with a Curie temperature larger than 1100 K [5]. The lattice parameter matches that of GaAs. Therefore, $Co_2FeSi$ is a suitable material for spin injection into GaAs-based structures such as for example spin light-emitting diodes (spin-LEDs [6–9]) and spin field effect transistors [10]. Samples produced by radio frequency magnetron sputtering have shown magnetically dead layers near the interfaces [11]. An epitaxial growth technique like molecular-beam epitaxy (MBE) may overcome these difficulties.

Recent theoretical studies indicate that a {111} interface may be superior to {001} interfaces with respect to the half-metallic properties of $Co_2FeSi$ [12]. Moreover, reacted compounds sometimes developing during $Co_2FeSi$ growth on GaAs(001) are bounded by {111} planes [13]. This observation led to the hypothesis that a {111} interface would be more stable. At the same time, reduced diffusion is expected perpendicular to the interface during growth on GaAs(111)B.

X-ray and electron diffraction experiments yield information about structure and long-range order of Heusler alloys and related materials [14–19]. In this study MBE grown $Co_2FeSi$/GaAs(111)B hybrid structures are investigated by transmission electron microscopy (TEM), x-ray diffraction, secondary ion mass spectometry (SIMS), and atomic force microscopy (AFM) in order to characterize the structural properties and the stability of the ferromagnet/semiconductor (FM/SC) interface and the $Co_2FeSi$ film. The growth mode of the epitaxial film [20, 21] is expected to have a fundamental influence on its structural properties. $Fe_3Si$ is a material very similar to $Co_2FeSi$ and grows on GaAs in the three-dimensional island (Volmer-Weber) growth mode [22, 23].

## II. STRUCTURE FACTORS OF THE $L2_1$ LATTICE

Fully ordered $Co_2FeSi$ crystallizes into the face centered $L2_1$ structure. This structure can be viewed as an fcc lattice with a basis consisting of four atoms A, B, C, and D with coordinates A(0, 0, 0), B(0.25, 0.25, 0.25), C(0.5, 0.5, 0.5), and D(0.75, 0.75, 0.75). In the ordered $Co_2FeSi$ crystal, Co atoms occupy two sublattices A, C, and Fe is on sublattice

B, while Si atoms fill the sublattice D. The degree of disorder can be described by three order parameters $\alpha$, $\beta$, and $\gamma$. $\alpha$ and $\beta$ are fractions of Si atoms occupying the Fe(B) and Co(A,C) sites, respectively [14, 15, 24]. $\gamma$ is defined as the number of Co atoms on Fe(B) sites. However, Fe and Co atoms cannot be distinguished by TEM, because they have very similar scattering factors ($f_{\mathrm{Fe}} \approx f_{\mathrm{Co}}$). In this approximation the second terms of the sums (2) and (3) are equal to zero. Then three types of reflections are expected for such a lattice: Fundamental reflections (not sensitive to disorder) and the two kinds of superlattice reflections arising due to long-range order. Fundamental reflections are not influenced by disorder. They are given by the rule $H + K + L = 4n$, where $n$ is an integer. One example for a fundamental reflection is 444. The structure amplitude is given by

$$F_{444} \propto (f_{\mathrm{Si}} + f_{\mathrm{Fe}} + 2f_{\mathrm{Co}}), \tag{1}$$

where $f_{\mathrm{Si}}$, $f_{\mathrm{Fe}}$, $f_{\mathrm{Co}}$ are atomic scattering factors of the respective elements. There are two distinct types of superlattice reflections [14, 15]. Reflections with odd $H, K, L$ like the 111 reflection are sensitive to two types of disorder (in the Fe(B) and Co(A,C) sublattices with the corresponding order parameters $\alpha$ and $\beta$), the structure amplitude being

$$F_{111} \propto (1 - 2\alpha - \beta)(f_{\mathrm{Fe}} - f_{\mathrm{Si}}) + (\gamma - \beta)(f_{\mathrm{Co}} - f_{\mathrm{Fe}}). \tag{2}$$

Reflections satisfying the condition $H + K + L = 4n - 2$ are sensitive only to disorder in the Co(A,C) sublattice, an example is 222 with the structure amplitude

$$F_{222} \propto (1 - 2\beta)(f_{\mathrm{Co}} - f_{\mathrm{Si}}) + (1 - 2\gamma)(f_{\mathrm{Co}} - f_{\mathrm{Fe}}). \tag{3}$$

Compared to the fully ordered $L2_1$ phase, the $B2$ phase is obtained by a complete mixing between the Fe and the Si atoms in the $Co_2FeSi$ lattice. The Co(A,C) sublattice remains fully ordered in this case, $\beta = 0$, and an intense (222) reflection is expected, see equation (3).

## III. EXPERIMENTAL

The structures were grown by solid-source MBE. The growth procedure on GaAs(001) is described in detail in Refs. [25, 26]. In our case GaAs(111)B samples with a 50-nm-thick GaAs buffer layer and an As-stabilized, (2×2)-reconstructed surface were grown first on a GaAs(111)B substrate and then transferred to an As-free growth chamber, in which

stoichiometric ≈ 15 nm thick $Co_2FeSi$ films were grown on top for different substrate temperatures $T_S$ ranging between $T_S = 100\,°C$ and $425\,°C$. (The nominal film thickness was slightly increased to 23 nm only for the maximum growth temperature $T_S = 425\,°C$.) Co, Fe, and Si are co-deposited from high-temperature effusion cells. The evaporation rates are controlled by the cell temperatures and are in accordance with the optimized fluxes for the growth of stoichiometric $Co_2FeSi$ films on GaAs(001) substrates [25]. The growth rate was approximately one monolayer in three minutes. The base pressure was about $1 \times 10^{-10}$ Torr. The growth was monitored by *in-situ* reflection high energy electron diffraction (RHEED). The samples were investigated by dark-field and high-resolution (HR) TEM. For that purpose cross-sectional TEM specimens were prepared by mechanical lapping and polishing, followed by argon ion milling according to standard techniques. TEM images were acquired with a JEOL 3010 microscope operating at 300 kV. In addition, X-ray measurements of diffraction and reflectivity were performed in a Panalytical X'Pert diffractometer equipped with a Ge (220) hybrid monochromator using $CuK\alpha_1$ radiation. Some of the samples were characterized by *ex-situ* AFM almost immediately after the growth. A Digital Instrument Nanoscope was utilized for this purpose. Depth profiles of the film constituents inside the GaAs buffer layer were determined by SIMS. The $Co_2FeSi$ layer was removed by selective wet chemical etching prior the SIMS profiling. The SIMS measurements were performed with a CAMECA IMS4F system.

## IV. NON-DESTRUCTIVE CHARACTERIZATION

Figure 1 shows high-resolution x-ray diffraction curves near the (222) diffraction peak of some of the samples investigated. Besides the narrow quasi-forbidden GaAs reflection, the broader $Co_2FeSi$ maximum is pronounced together with thickness fringes. Those fringes indicate a smooth FM/SC interface and and a high quality surface of the film, similar to the results of x-ray reflectivity measurements. The observation of an intense (222) reflection indicates a perfect epitaxial growth with a Co(A,C) sublattice almost free of Si atoms ($\beta \approx 0$), see equation (3). That means the $Co_2FeSi$ film shows at least a $B2$ ordering, i.e. the Si atoms are mixed preferably with the Fe atoms ($\alpha > 0$). Some modifications of the diffraction curves are found. In the case of $T_S = 325$ °C the thickness fringes are less pronounced due to a degradation of surface and interface quality. For $T_S = 425$ °C a shift of the $Co_2FeSi$

peak is observed and the thickness fringes vanish probably due to an additional change in stoichiometry of the film.

The $Co_2FeSi$ surface after growth at $T_S = 100\,^{\circ}C$ imaged by atomic force microscopy is quite smooth with a terrace size of about one $\mu$m, see Fig. 2 (a). The pattern of the steps is similar to that of a GaAs(111)B surface. Some triangular islands are visible on the broad terraces. For higher growth temperatures a slight deterioration of the surface is found, although the root mean squared (RMS) roughness is limited to values below 0.5 nm for growth temperatures up to $T_S = 275\,^{\circ}C$, Fig. 2 (b).

## V. TEM CHARACTERIZATION

### A. The $Co_2FeSi$/GaAs(111)B interface

Figure 3 shows a cross-section HRTEM micrograph (Fourier filtered) along the GaAs $[2\bar{1}\bar{1}]$ zone axis of a sample grown at $T_S = 100\,^{\circ}C$ and a corresponding selected area diffraction pattern illustrating the cube-on-cube orientational relationship between $Co_2FeSi$ and GaAs. All the diffraction maxima of $Co_2FeSi$ and GaAs overlap fully due to the small misfit between stoichiometric $Co_2FeSi$ and GaAs. For all samples investigated, the orientational relationship (111)GaAs $\parallel$ (111)$Co_2FeSi$ and $\langle 110\rangle$GaAs $\parallel$ $\langle 110\rangle Co_2FeSi$ was established. The interface between the $Co_2FeSi$ film and the GaAs buffer layer is smooth and distributed only over a few monolayers. The samples grown at $T_S = 225\,^{\circ}C$ and at $T_S = 275\,^{\circ}C$ were free of interface reactions as well. For $T_S = 275\,^{\circ}C$ we could observe some additional phenomena: In the HRTEM micrograph (Fig. 4) a slight modification of the interface with a roughness of 0.8 nm (see e.g. the region between the dashed lines) is visible together with typical inhomogeneities (marked by full lines) of the $Co_2FeSi$ films. The origin of these inhomogeneities will be explained in section (V.C.). Disk shaped precipitates produced by interfacial reactions were detected by cross-sectional TEM for all samples grown at $T_S \geq 325\,^{\circ}C$. Additionally, we found peaks in x-ray diffraction curves caused by the interface reaction products. MBE growth of $Co_2FeSi$ on GaAs(001) resulted in an interface reaction at $T_S = 250\,^{\circ}C$, while a modification of the interface already took place at $T_S = 200\,^{\circ}C$ , cf. [13, 25]. So, the $Co_2FeSi$/GaAs(111)B hybrid structures are stable at temperatures 75 K higher than $Co_2FeSi$/GaAs(001) structures in agreement with our expectation mentioned in the intro-

duction.

Figure 5 (a) is a multi-beam cross-section TEM micrograph at lower magnification along the GaAs $[2\bar{1}\bar{1}]$ zone axis of a $Co_2FeSi$ film grown on GaAs at $T_S = 325\,^{\circ}C$. A large reacted region (lower edge marked by dotted line) is visible below the $Co_2FeSi$/GaAs(111) interface. Figure 5 (b) is a higher magnification of one part of (a) illustrating the degradation of the interface in the immediate vicinity of the precipitate. The precipitates in the samples grown at $T_S = 325\,^{\circ}C$ are always platelets at the interface. They are detected in the GaAs buffer layer, and their predominant boundary is (111). A typical lateral size of these precipitates is ≈100 nm, whereas their extent perpendicular to the interface is about 10–20 nm. Precipitates in samples grown at $T_S = 425\,^{\circ}C$ are even larger and have irregular shapes. The distance between the precipitates is of the order of micrometers. The remaining part of the FM/SC interface between the precipitates is almost perfect and may still contribute to an effective spin injection into the semiconductor device. Earlier observations [9] have shown for a similar system, namely for $Co_2FeSi$/(Al,Ga)As spin LEDs grown on GaAs(001) substrates at high $T_S$, a high spin injection efficiency inspite of the presence of precipitates. The morphology of the reacted regions near the (111) interface is clearly different from the appearance of the precipitates found in samples grown on GaAs(001) [13]. In our case the precipitates are larger and more flattened along the (111) interface. Therefore (111) boundaries seem to act as barriers for diffusion-driven precipitate formation.

### B. Long-range order in $Co_2FeSi$

Figure 6 shows a selected area electron diffraction pattern of the $Co_2FeSi$ film along the $[01\bar{1}]$ direction. We see a rectangular grid of the fundamental reflections (indexed, see red line) and a less intense hexagonal grid (see black line) of superlattice reflections in the vicinity. We have the choice to image our sample in any of those reflections. Figure 7 shows e.g. a comparison of two dark-field micrographs: taken (a) with the (444) fundamental reflection (not sensitive to disorder of the $Co_2FeSi$), and (b) with the (111) superlattice reflection (sensitive to disorder).

Let us first consider the image of the GaAs buffer layer: On the GaAs side of the interface we see in (a) and (b) an inhomogeneous stripe caused by strain connected to diffusion of film atoms into the GaAs buffer layer. This diffusion was also detected by SIMS depth profiling,

as shown in Fig. 8 for the example of Co in-diffusion. The maximum Co concentration in the uppermost part of the GaAs is almost constant up to a temperature of $T_S = 275\,^{\circ}\mathrm{C}$ and then increases drastically for the higher growth temperatures. Similar results are obtained for the Fe and Si depth profiles (not shown here): However, the Fe concentrations are about one order of magnitude lower and the Si concentrations two orders of magnitude lower than the corresponding Co concentration, i.e. a very rough estimate of stoichiometry of the in-diffused material is given by the formula $Co_{100}Fe_{10}Si$. For $T_S \leq 325\,^{\circ}\mathrm{C}$, a maximum in the Co concentration is found at approximately 20 nm below the interface, which is in good agreement with the observation in Fig. 7. A Co concentration depth profile below a $Co_2FeSi$ layer grown on GaAs(001) at $T_S = 275\,^{\circ}\mathrm{C}$ is also included in Fig. 8. However, the diffusion of Co into the GaAs in this case is strongly enhanced by almost one order of magnitude compared to the films grown on GaAs(111)B at the same $T_S$ verifying the reduced diffusion activity perpendicular to the (111) plane.

Now let us consider the image of the $Co_2FeSi$ film: The (444) reflection shown in Fig. 7 (a) is a fundamental reflection for the $Co_2FeSi$ lattice, i.e. it is not sensitive to disorder. The disorder-sensitive superlattice (111) reflection is imaged in Fig. 7 (b) [15, 16]. Under the condition, that the TEM micrograph with g = 444 is homogeneous the micrograph taken with g = 111 reveals the spatial distribution of long-range order. It shows brighter areas, that are due to well ordered regions in the film. These ordered regions are not distributed uniformly. Moreover a darker stripe is found near the interface, i.e. near the interface the lattice is ordered to a lesser extent. The image of the $Co_2FeSi$ (111) reflection is less homogeneous and less intense than the image of the fundamental $Co_2FeSi$ (444) reflection shown in Fig. 7(a). The striking difference in intensity of both reflections (the GaAs intensity should be taken into account as a reference for a comparison) can be explained by their different structure factors, see equations (1) and (2). We estimated the order parameters from x-ray diffraction results by comparison of the integrated intensities of the fundamental and superlattice film reflections [17]. (The substrate reflections were used as an internal reference.) Approximately 25% of the Si atoms left their sublattice (sample grown at $T_S = 275\,^{\circ}\mathrm{C}$) and changed positions with the Fe atoms. For such a disorder the $Co_2FeSi$ (444) reflection is expected to be more than 50 times more intense than the $Co_2FeSi$ (111) reflection, a value, which seems to be in a reasonable agreement with Fig. 7.

Next we consider the long-range order of a film grown at higher temperature: Figure 9

shows a HRTEM micrograph of a sample grown at $T_S = 425\,^{\circ}C$. Here we see an area with clearly dominant well ordered $L2_1$ phase in the $Co_2FeSi$ film (honeycomb-like contrast, inset: image simulation, performed with the program Electron Microscopy Image Simulation, EMS On Line, http://cecm.insa-lyon.fr/CIOL/). Only the region very near to the FM/SC interface consists of the $B2$ phase (fringe contrast). This example demonstrates that the long-range order of the $Co_2FeSi$ lattice is improved for the samples grown at higher $T_S$.

### C. Origin of inhomogeneities

In the micrograph shown in Fig. 10 , we observe well distinguished grains in the film grown at $T_S = 425\,^{\circ}C$ originating from island growth of $Co_2FeSi$ on GaAs(111)B and the coalescence of those islands. Grains of different orientation produce different interference patterns (phase contrast) in the HRTEM micrograph. Additional tilt or twist of the grains modify these patterns. In the micrograph, one of the grains seems darker and exhibits a modulated phase contrast, which is probably caused by a slight tilt or twist of that grain with respect to its neighbors. In other regions, these modulation stripes are found to be perpendicular to the FM/SC interface pointing to a lateral strain in the grains. The inhomogeneity in the HRTEM micrograph shown in Fig. 4 resembles the grain structure of the film grown at $T_S = 275\,^{\circ}C$, whereas Fig. 11 shows the grain structure of a film grown at $T_S = 100\,^{\circ}C$. While the GaAs substrate diffracts homogeneously, we see an inhomogeneous contrast in the micrograph of the film, probably caused by residual strain in the different grains. Such a strain could be caused by a local change in stoichiometry, which is always accompanied by a change in the lattice parameter [25]. A change in local stoichiometry may be due to a lateral segregation or stress relaxation near the step edges of the GaAs surface. Despite a small misfit between the $Co_2FeSi$ film and the GaAs buffer layer, the observed formation of grains in the film is evidence for three-dimensional (3D) island growth during the first stage of heteroepitaxy of $Co_2FeSi$ on GaAs(111)B before a continuous film is formed. Such island growth is caused by the higher surface tension of the metal compared to the semiconductor substrate. Indeed the surface tension of the metals Fe and Co is relatively high [27]. The surface tension of $Co_2FeSi$ is similar to that of $Fe_3Si$, for which the Volmer-Weber (3D island) growth mode was observed on GaAs(001) earlier using *in-situ* x-ray diffraction [22, 23]. The difference of the surface tension $\Delta\sigma_1$ of $Fe_3Si$ and $Co_2FeSi$ should

be small compared to the difference $\Delta\sigma_2$ of GaAs and $Co_2FeSi$ ($\Delta\sigma_1 \ll \Delta\sigma_2$) leading us to the expectation of an 3D island growth mode of $Co_2FeSi$ on GaAs(111)B. However, in-situ RHEED measurements did not detect a roughening of the surface indicating relatively large and very flat islands. Our growth rate one monolayer in three minutes is very near to a simulated kinetic optimum of 3D island growth with a resulting RMS surface roughness of less than one monolayer during all stages of the growth, see kinetic Monte Carlo simulations in [22]. Under this condition RHEED would show a smooth surface.

In our case the spatial distribution of the long-range order in Fig. 7(b) is similar to the distribution of grains shown in Figs. 10 and 11. The origin of these grainy inhomogeneities in the long-range order probably lies in a segregation at step edges or a local strain relaxation of the the $Co_2FeSi$ film (without formation of misfit dislocations) via non-stoichiometry (with a formation and movement of point defects) leading to a local change in the lattice. In one way or the other neighboring grains would have a slightly different lattice parameter. No extended defects are needed for these inhomogeneities. A change in stoichiometry of the the $Co_2FeSi$ film could arise as a consequence of the diffusion into the GaAs buffer layer as well. Obviously inhomogeneity of the stoichiometry is directly related to an inhomogeneity in the long-range ordering. During the epitaxial growth the islands nucleate independently and randomly on the GaAs surface, grow and eventually coalesce. In this way the local growth conditions in each of the grains influence long-range order in this grain, e.g. due to different sticking of the $Co_2FeSi$ film atoms at step edges or simply due to a slight change in stoichiometry driven by inhomogeneity of local mismatch.

## VI. CONCLUSION

$Co_2FeSi$ films on GaAs(111)B grow in the Volmer-Weber 3D island growth mode, contain the ordered $L2_1$ phase, and have a stable interface up to $T_S = 275$ °C, a growth temperature which is 75 K higher than the temperature guaranteeing a stable interface during growth on GaAs(001). The distribution of long-range order in the $Co_2FeSi$ films was characterized by comparison of the dark-field TEM images taken in a homogeneous fundamental reflection and an inhomogeneous superlattice reflection. The spatial inhomogeneities in the long-range order resemble the grainy structure of the $Co_2FeSi$ film. These inhomogeneities are arising during the growth of the islands and their coalescence via a local change in stoichiometry,

which can lead to a relaxation of local strain without formation of extended defects.

## VII. ACKNOWLEDGEMENT

The authors thank Hans-Peter Schoenherr for his support during the MBE growth, Doreen Steffen for sample preparation, Astrid Pfeiffer for help in the laboratory, Esperanza Luna and Vladimir Kaganer for valuable support and helpful discussion.

---

[1] C. Felser and B. Hillebrands, J. Phys. D: Appl. Phys. **42**, 080301 (2009).

[2] G. A. Prinz, Science **282**, 1660 (1998).

[3] A. Fert, Thin Solid Films **517**, 2 (2008).

[4] I. Zutić, J. Fabian, and S. D. Sarma, Rev. of Mod. Phys. **76**, 323 (2004).

[5] S. Wurmehl, G. H. Fecher, H. C. Kandpal, V. Ksenofontov, C. Felser, H.-J. Lin, and J. Morais, Phys. Rev. B **72**, 184434 (2005).

[6] Y. Ohno, D. K. Young, B. Beschoten, F. Matsukura, H. Ohno, and D. D. Awschalom, Nature **402**, 790 (1999).

[7] H. J. Zhu, M. Ramsteiner, H. Kostial, M. Wassermeier, H.-P. Schönherr, and K. H. Ploog, Phys. Rev. Lett. **87**, 016601 (2001).

[8] A. T. Hanbicki, B. T. Jonker, G. Itskos, G. Kioseoglou, and A. Petrou, Appl. Phys. Lett. **80**, 1240 (2002).

[9] M. Ramsteiner, O. Brandt, T. Flissikowski, H. T. Grahn, M. Hashimoto, J. Herfort, and H. Kostial, Phys. Rev. B **78**, 121303 (2008).

[10] S. Sugahara and M. Tanaka, Appl. Phys. Lett. **84**, 2307 (2004).

[11] M. Kallmayer, H. J. Elmers, B. Balke, S. Wurmehl, F. Emmerling, G. H. Fecher, and C. Felser, J. Phys. D: Appl. Phys. **39**, 786 (2006).

[12] J. J. Attema, G. A. de Wijs, and R. A. de Groot, J. Phys. D: Appl. Phys. **39**, 793 (2006).

[13] M. Hashimoto, J. Herfort, A. Trampert, H.-P. Schönherr, and K. H. Ploog, J. Phys. D: Appl. Phys. **40**, 1631 (2007).

[14] P. J. Webster, J. Phys. Chem. Solids **32**, 1221 (1971).

[15] V. Niculescu, K. Raj, J. I. Budnick, T. J. Burch, W. A. Hines, and A. H. Menotti, Phys. Rev. B **14**, 4160 (1976).

[16] V. Niculescu, J. I. Budnick, W. A. Hines, K. Raj, S. Pickard, and S. Skalski, Phys. Rev. B **19**, 452 (1979).

[17] B. Jenichen, V. M. Kaganer, J. Herfort, D. K. Satapathy, H. P. Schönherr, W. Braun, and K. H. Ploog, Phys. Rev. B **72**, 075329 (2005).

[18] S. Wurmehl, G. H. Fecher, H. C. Kandpal, V. Ksenofontov, C. Felser, and H.-J. Lin, Appl. Phys. Lett. **88**, 032503 (2006).

[19] Y. Takamura, R. Nakane, and S. Sugahara, J. Appl. Phys. **105**, 07109 (2009).

[20] E. Bauer, Z. Kristallographie **110**, 372 (1958).

[21] J. Y. Tsao, *Materials Fundamentals of Molecular Beam Epitaxy* (Academic Press, Inc., San Diego, CA, 1992).

[22] V. M. Kaganer, B. Jenichen, R. Shayduk, W. Braun, and H. Riechert, Phys. Rev. Lett. **102**, 016103 (2009).

[23] B. Jenichen, V. M. Kaganer, R. Shayduk, W. Braun, and A. Trampert, Phys. Stat. Sol. A **206**, 1740 (2009).

[24] Y. Takamura, R. Nakane, and S. Sugahara, Cond-mat/1002.1564 (2010).

[25] M. Hashimoto, J. Herfort, H.-P. Schönherr, and K. H. Ploog, Appl. Phys. Lett. **87**, 102506 (2005).

[26] M. Hashimoto, J. Herfort, H.-P. Schönherr, and K. H. Ploog, J. Appl. Phys. **98**, 104902 (2005).

[27] A. Zangwill, *Physics at Surfaces* (Cambridge University Press, Cambridge, UK, 1988).

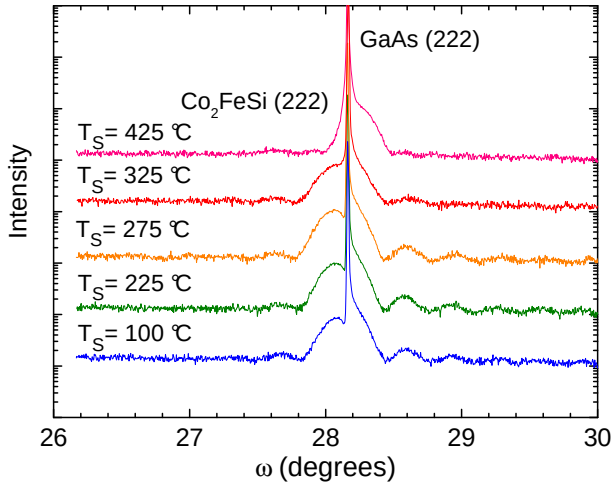


Figure 1. High resolution x-ray diffraction curves measured near the GaAs (222) reflection of samples grown at different substrate temperatures $T_S$. The narrow peak is the quasiforbidden GaAs reflection and the broader maximum is the $Co_2FeSi$ (222) superlattice reflection indicating at least a $B2$ ordering of all the films. The thickness fringes demonstrate a high quality of the FM/SC interface and surface.

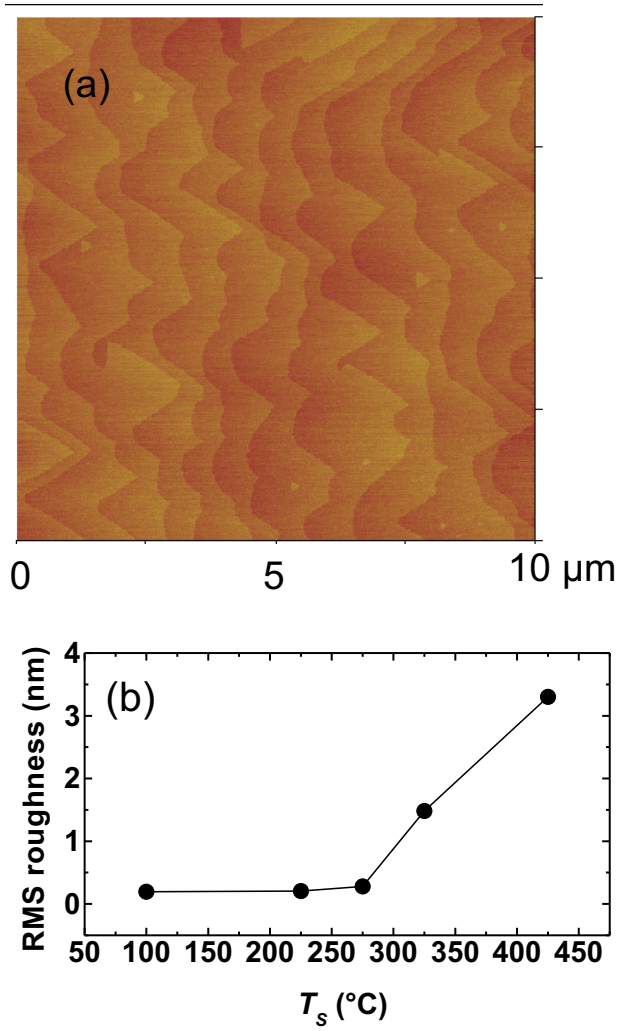


Figure 2. (a) AFM micrograph of the $Co_2FeSi$ surface grown on GaAs(111)B at $T_S$= 100 °C. (b) Root mean squared (RMS) surface roughness in dependence of the growth temperature of the samples.

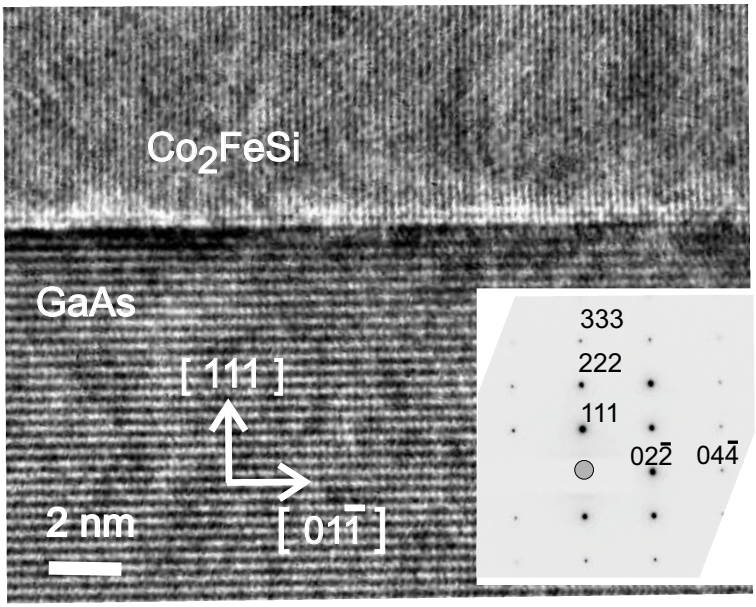


Figure 3. Cross-section HRTEM micrograph (Fourier filtered) along the GaAs $[2\bar{1}\bar{1}]$ zone axis of a sample grown at $T_S = 100\,^{\circ}\mathrm{C}$ and a corresponding selected area diffraction pattern illustrating the orientational relationship between $Co_2FeSi$ and GaAs. Due to the vanishing misfit between stoichiometric $Co_2FeSi$ and GaAs, their diffraction maxima fully coincide. The interface is smooth.

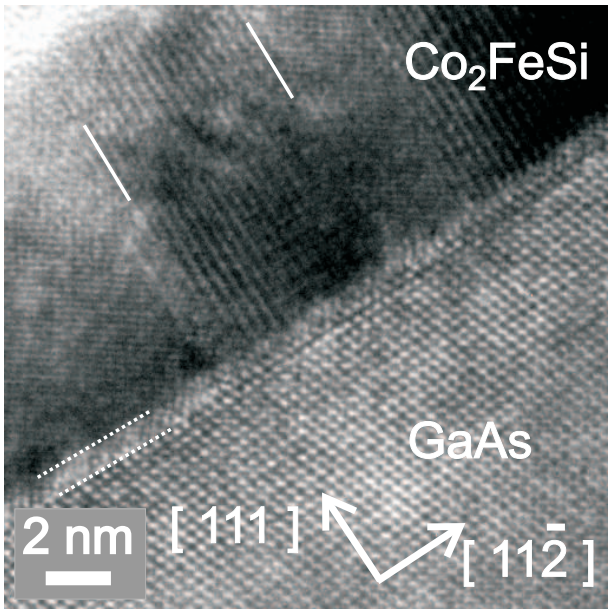


Figure 4. Cross-section HRTEM micrograph along the GaAs [01$\bar{1}$] zone axis of a sample grown at $T_S = 275\,^{\circ}$C. The FM/SC interface has a roughness of 0.8 nm (see region between dashed lines) compared to those of samples grown at lower $T_S$. Inhomogeneities of the $Co_2FeSi$ film are visible (marked by full lines).

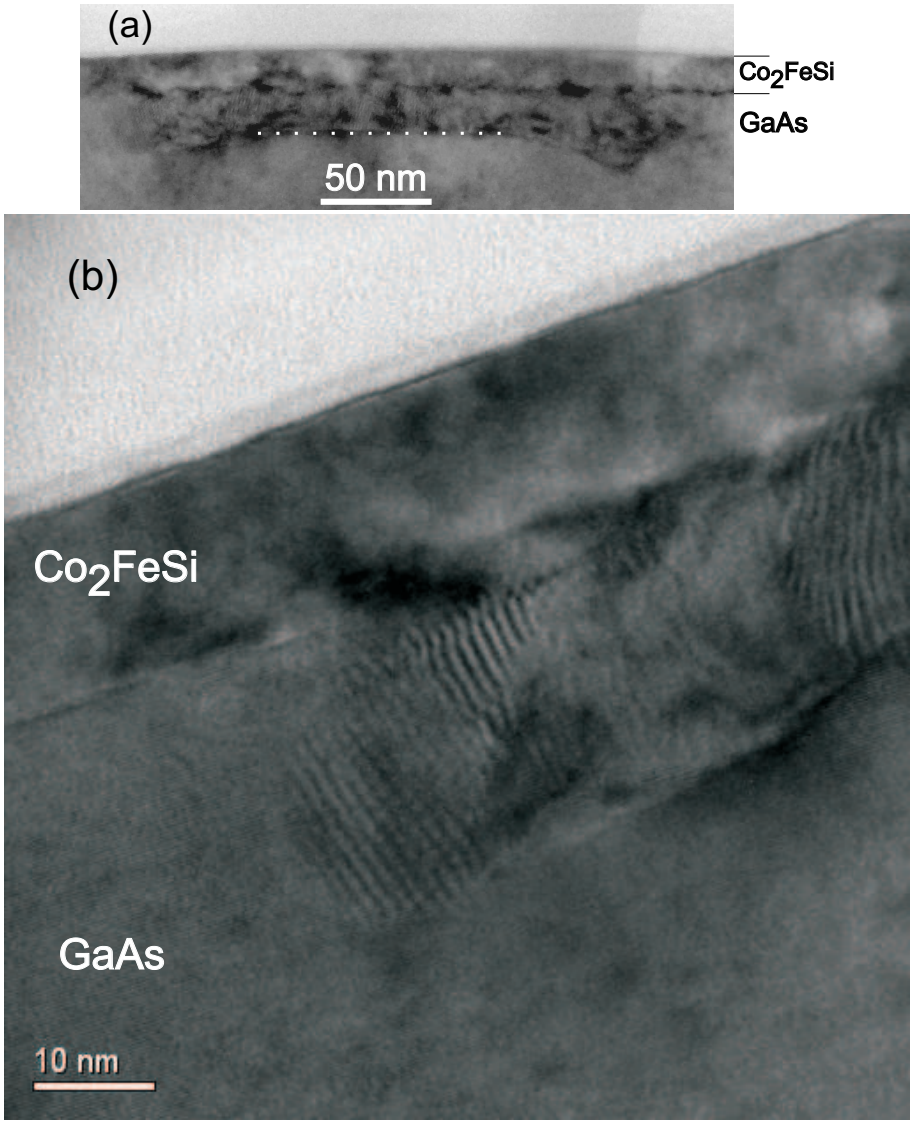


Figure 5. Cross-section multi-beam TEM micrograph along the GaAs $[2\bar{1}\bar{1}]$ zone axis of a $Co_2FeSi$ film grown on GaAs at $T_S = 325\,^{\circ}C$. In (a) a large reacted region (lower edge marked by dotted line) is visible below the $Co_2FeSi$/GaAs(111) interface . (b) is a magnification of the region near the left end of the precipitate.

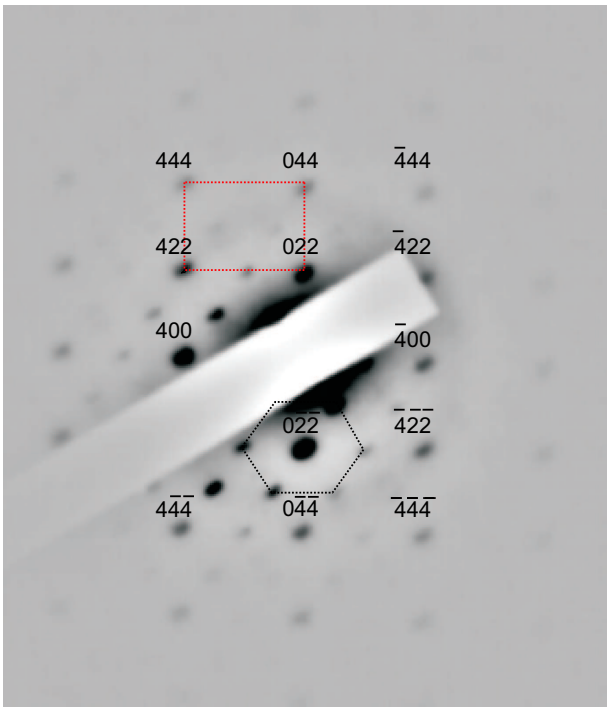


Figure 6. Selected area diffraction pattern along the $Co_2FeSi/GaAs$ $[01\bar{1}]$ zone axis of a sample grown at $T_S = 275\,°C$. A rectangular pattern of $Co_2FeSi$ fundamental reflections (indexed, red dashed line) of the $L2_1$ structure is observed. This rectangular pattern is slightly more pronounced than the hexagonal pattern (black dashed line) of the superlattice maxima in the vicinity.

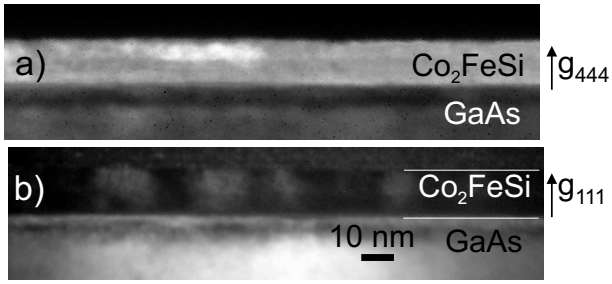


Figure 7. Dark-field cross-section TEM micrographs of the sample grown at $T_S = 275\,°C$. a) The fundamental $Co_2FeSi$ (444) reflection diffracts quite intensively and homogeneously. b) The image of the $Co_2FeSi$ (111) superlattice reflection of the same region is less intense and less homogeneous. On the GaAs side of the FM/SC interface both reflections reveal contrasts due to lattice strain connected to diffusion into the GaAs substrate.

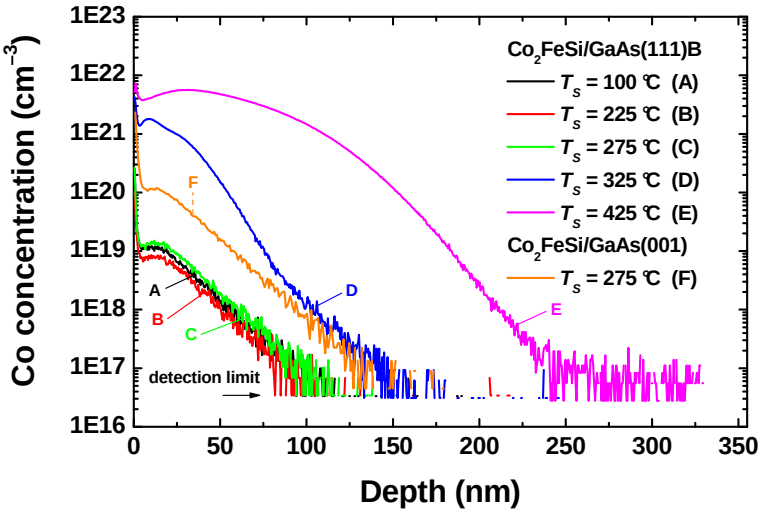


Figure 8. SIMS depth profiles for Co in-diffusion at different growth temperatures of the $Co_2FeSi$ layers. The GaAs buffer layer starts at a depth of zero and ends at 50 nm, because the $Co_2FeSi$ was removed before the SIMS measurement by etching.

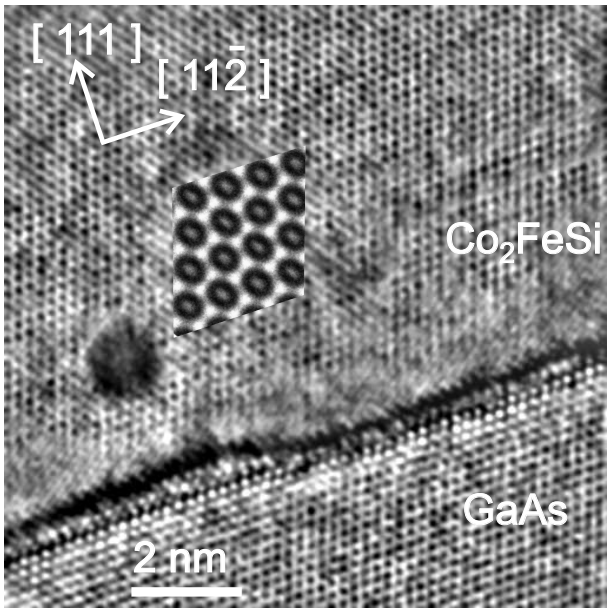


Figure 9. Cross-section HRTEM micrograph (Fourier filtered) along the GaAs $[01\bar{1}]$ zone axis of a sample grown at $T_S = 425\,^{\circ}\mathrm{C}$. Here the dominant $L2_1$ phase of $Co_2FeSi$ is observed more far from the interface (inset: simulation), whereas the $B2$ phase (fringed contrast) is seen near the interface.

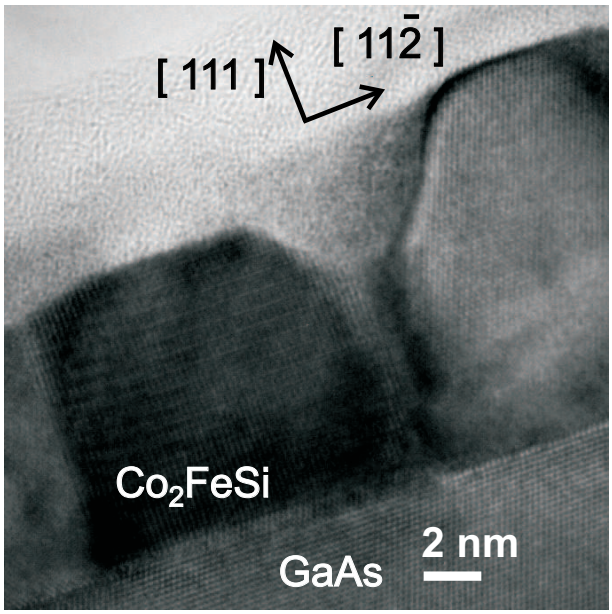


Figure 10. Cross-section HRTEM micrograph along the GaAs [01$\bar{1}$] zone axis of a sample grown at $T_S = 425\,^{\circ}\mathrm{C}$. Different grains can be distinguished clearly and for one grain a modulated contrast pattern is observed. Obviously the grains were formed after coalescence of islands. The shape of the former islands is visible from the shape of the $Co_2FeSi$ surface.

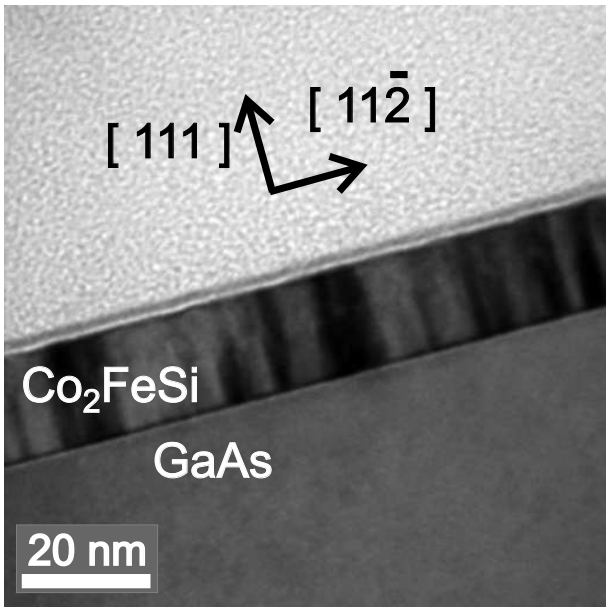


Figure 11. Cross-section multi-beam TEM micrograph at lower magnification along the GaAs [01$\bar{1}$] zone axis of a sample grown at $T_S = 100\,^{\circ}\mathrm{C}$. Different grains can be distinguished due to changing contrast in the micrograph. The GaAs substrate diffracts homogeneously.